Special Issue on "Theoretical and Computational Chemistry"

J. Indian Chem. Soc.,
Vol. 96, July 2019, pp. 933-947

Does semihydrogenated graphene on lattice matched transition metal substrates has a uniform hydrogen adsorption pattern?

Niharika Joshi[a]* and Prasenjit Ghosh[b]

[a]Department of Chemistry, [b]Department of Physics and Center of Energy Sciences,

Indian Institute of Science Education and Research Pune, Pune-411 008, Maharashtra, India

E-mail: niharika.joshi@students.iiserpune.ac.in

Manuscript received online 07 May 2019, revised and accepted 13 May 2019

Graphone, uniformly semihydrogenated graphene, though an interesting material, is known to be highly unstable due to large chemical imbalance between the sublattices of the bipartite graphene lattice. The freestanding semihydrogenated graphene (GrH) sheet can be stabilized by changing the hydrogen adsorption pattern in such a way that the chemical imbalance is removed. However, when placed on lattice-matched transition metal surfaces we find that the highly unstable uniformly semihydrogenated graphene is stabilised and on Ni(111) surface it shows equal stability with at least three other structures. The other three structures are rectangular graphone, zigzag graphone and armchair graphone. On Co(111) and Cu(111) surfaces rectangular graphone shows more stability than other structures. Nonetheless the corelevel shifts of these four semihydrogenated graphene on the (111) surfaces of Ni, Co and Cu shows differences which are less than 0.2 eV. It is thus highly unlikely that X-ray Photoelectron spectroscopy measurements will be able to discern different H adsorption patterns. Therefore our study contradicts the notion that upon hydrogenation of graphene sheet supported on a lattice matched transition metal substrates a uniform H adsorption pattern will be formed. Furthermore we find that the electronic and magnetic properties at the interface of semihydrogenated graphene and metal surface show variation with H adsorption patterns. This makes the study of hydrogenated graphene on transition metal surfaces more intriguing and important from the point of view of using the interface as a device. Of all structures studied in this paper we find that only uniform graphone on Cu(111) surface shows higher possibility for spin polarized conduction at the interface.

Keywords: Semihydrogenated graphene, sublattice imbalance, core-level shift.

1. Introduction

Chemical modifications through hydrogenation of graphene is one of the most popular ways to alter its properties. First principles study by Zhou *et al.*[1] predicted that a freestanding uniformly semihydrogenated graphene sheet (UGrH) is ferromagnetic. However, it is highly unstable due to the sublattice imbalance induced in the graphene sheet. The sublattice imbalance is defined as, $\eta = N_\alpha - N_\beta$, where N_α and N_β are number of C atoms at sublattices α and β in graphene respectively, to which the adsorbing species binds. Zero sublattice imbalance implies $\eta = 0$. It is observed that the sublattice imbalance is minimized, and hence stability is enhanced, when H atoms are absorbed in a more closed packed pattern on the graphene sheet[2,3]. Clustering of H was observed experimentally using scanning tunnelling microscopy (STM) studies at both low and high H exposures on the epitaxial graphene sheet supported on SiC substrate[4]. Different first principles studies, through simulations of diffusion of atomic H from the UGrH structure, were able to predict H adsorption patterns of GrH with zero chemical imbalance, that are found to be more stable than UGrH. Feng *et al.*[5] predicted a rectangular arrangement (RGrH) while Šljivančanin *et al.*[6] suggested a zigzag arrangement (ZGrH) of H atoms on the semihydrogenated graphene sheet. Hence it would be interesting to explore whether there are other possible H adsorption patterns with $\eta = 0$ and whether there is ground state structure for freestanding semihydrogenated graphene.

Another way to reduce the sublattice imbalance is to synthesize GrH on a substrate like transition metal (TM) surfaces. The interaction of graphene divides TM surfaces into two groups: (i) metal surfaces on which graphene is chemisorbed like Ni, Co, Rh, Ru and (ii) metal surfaces on which graphene is physiorbed like Cu, Au, Ag, Ir, Pt[7–9]. Furthermore each groups can be further divided into subgroups: (1) the metal surfaces with lattice parameter in close agreement with that of graphene (2.46 Å) like Ni(111) (2.49 Å), Co(0001) and Co(111) (2.51 Å) from group (i) and Cu (2.6 Å) from group (ii) and (2) the metal surface which have large lattice mismatch with graphene [for example Rh(0001) and Ru(111) from group (i) and (111) surfaces of Ir, Pt, Au from group (ii)]. On lattice mismatched metal surfaces it is observed that between two successive top-site C atoms along the lattice vectors of the metal surface the positions of the C atoms vary continuously from top site to bridge site to top site. The top site is defined as when the C atom sits right atop of the surface metal atom while bridge site is defined when the C-C bond is on the top or hollow site of the metal surface. The relative change in the position of C atoms causes periodic buckling in graphene sheet such that some portions of the graphene sheet show binding to metal substrate while some do not. The hydrogenation pattern on the supported graphene sheet is observed to be sensitive to the interaction of epitaxial graphene with its substrate. For example High Resolution Electron Energy Loss Spectroscopy (HREELS) studies of Kyhl *et al*.[10] have shown that the graphane-like structures are formed where the carbon atoms in the graphene sheet interact strongly with the Ir(111) substrate, while dimer formation is observed at other sites that show weaker interactions. Further the degree of hydrogen uptake also varies depending on the substrate. For example, Son *et al*.[11] found that uptake of hydrogen is reduced by 50% when the graphene sheet is on hexagonal boron nitride (almost lattice matched with graphene) compared to that observed when the support is silicon or molybdenum disulphide (MoS_2). Similarly, among TM surfaces, graphene supported on lattice-mismatched Ir(111) and Pt(111) show large hydrogen uptake of around 67% and 50%[12]. In contrast, on commensurate Ni(111) surface, it is observed that the H uptake on graphene is only 17%[12]. Only recently Zhao *et al*.[13] have shown from their combined study using X-ray Photoelectron Spectroscopy (XPS) measurements and density functional theory (DFT) calculations that graphene sheet supported on Ni(111) surface can show an uptake of 50% H resulting in GrH. Based on their DFT studies they concluded that the adsorbed hydrogen form an uniform adsorption pattern, i.e. UGrH. The pattern formation observed upon H adsorption on the graphene sheet supported on surfaces of TM such as Ir and Pt are driven by the strain that the graphene sheet experiences due to lattice mismatch. However, on surface of TM like Ni, Co and Cu the C atoms of the graphene sheet is in registry with the substrate and there is negligible strain on graphene. On lattice matched surfaces the most stable configuration of graphene is where one of the C sublattice is on top of the metal atoms while the second one is at a hollow site[14–16]. Based on the concept of sublattice imbalance, it is natural to expect that the adsorbed H atoms form a uniform pattern, i.e. they bind only to the C atoms that are in registry with the hollow site of the metal surface. However, this gives rise to a set of questions such as (1) What happens to the other adsorption patterns, namely the ZGrH and RGrH, that were more stable compared to UGrH for the free standing GrH? (b) Can these or some other novel H adsorption patterns be stabilized for graphene on these substrates and if so, how their properties are affected because of the interaction with the substrates?

To find answers to these questions, we have investigated the relative thermodynamic stability and properties of semihydrogenated graphene with different H adsorption patterns on three transition metal surface, namely Ni(111) and Co(111) from group (i) and Cu(111) from group (ii). The rest of the paper is organized as follows. The details of the computational methods used in our study are given in Section 2. Then in Section 3 we present and discuss our results, first on freestanding and then on TM surface-supported semihydrogenated graphene. We also compare our results with the XPS measurements reported by Zhao *et al*.[13]. Finally, we summarize our results and conclude in Section 4

2. Computational method

We have performed *ab initio* spin polarized DFT calculations using plane-wave based Quantum ESPRESSO software[17] for investigating semihydrogenation of freestanding graphene and graphene supported on Ni(111), Co(111) and Cu(111) surfaces. The electron-ion interactions have been treated with ultrasoft pseudopotentials[18] that are available on Quantum ESPRESSO website[19]. The pseudopotentials have been generated using Rappe Rabe Kaxiras

Joannopoulos (RRKJ) method[20]. The valence configurations used for the generation of pseudopotentials for C, H, Ni, Co and Cu are [He]$2s^2$ $2p^2$, $1s^1$, [Ar]$4s^1$ $3d^9$, [Ar]$4s^1$ $3d^8$ and [Ar]$4s^1$ $3d^{10}$, respectively. The kinetic energy cutoffs for wavefunction and charge density used for the calculation in freestanding condition are 35 Ry and 280 Ry, respectively, those on Ni(111) and Cu(111) surface are 35 Ry and 360 Ry, respectively and those on Co(111) surface are 40 Ry and 320 Ry. The electron-electron exchange-correlation potential is described by Perdew, Burke and Ernzerhof parametrization which uses the generalized gradient approximation[21]. The Brillouin zone integrations are performed on a 12×12×1 Monkhorst Pack shifted k-point grid per (1×1) unit cell of graphene[23]. For speeding up the calculations we have used Marzari-Vanderbilt smearing[22] of widths 0.003 Ry and 0.01 Ry for the freestanding and supported semihydrogenated graphene, respectively.

Further we have tested the pseudopotentials by computing the following quantities: We have obtained the lattice parameter of Ni bulk to be 3.52 Å with magnetic moment of $0.64\mu_B$ per Ni atom; lattice parameter of Co bulk to be 2.50 Å and c/a ratio of around 1.55 with magnetic moment of $1.69\mu_B$ per Co atom; lattice parameter of Cu bulk to be 3.67 Å. For freestanding graphene, we have obtained the lattice parameter of 2.46 Å with C-C bond length of 1.43 Å. These preliminary results for TM bulk and pristine graphene are in excellent agreement with the previous reports[1,26]. Upon uniformly semihydrogenating graphene the sheet becomes buckled with the hydrogenated carbon moving out-of-plane. The buckling is obtained of around 0.32 Å, the C-C bond length increases to 1.50 Å and the C-H bond length is about 1.15 Å. The graphene sheet becomes ferromagnetic semiconductor with total magnetization of $1\mu_B$/(1×1) unit cell, which is majorly contributed by the unhydrogenated carbon atom, and an indirect bandgap of around 0.68 eV. These results for the uniformly semihydrogenated graphene or graphone are in perfect agreement with those reported by Zhou *et al.*[1].

Uniform graphone can be modeled in 1×1 hexagonal cell while zigzag, rectangular and armchair requires supercell of size 1×2, 2×1 and 2×2, respectively. In order to investigate all the different H adsorption patterns in the same size of cell we have modeled the graphene sheet in an orthorhombic unit cell whose optimized lattice parameters are a = 4.27 Å and b = 4.93 Å. Each unit cell contains 8 carbon atoms. The cell parameters are further optimized upon semihydrogenating the graphene sheet with different H adsorption patterns which are given in Table 1. On a substrate, the lattice parameter of graphene will be determined by that of the substrate. Hence, the semihydrogenated graphene supported on TM surfaces is modeled in the orthorhombic unit cell of (i) Ni(111) surface lattice with a = 4.32 Å and b = 4.98 Å; (ii) Co(111) surface lattice with a = 4.35 Å and b = 5.02 Å and (iii) Cu(111) surface lattice with a = 4.50 Å and b = 5.19 Å. The slab of (111) surface of Ni, Co and Cu are asymmetric and consist of 6, 7, 6 layers, respectively, of which bottom 3 layers are kept fixed at the bulk interplanar distance while the top 3 layers are relaxed. The periodic images of pristine graphene and clean TM surfaces in the direction perpendicular to the surface are separated by a vacuum of 12 Å thickness to minimize the spurious interaction between them. The interaction between TM surface and graphene is weak chemisorption in case of Ni(111) and Co(111) while physiorption in case of Cu(111) surface. Therefore for obtaining the TM-C interaction correctly at the interface one needs to consider the dispersion interaction between the two surfaces, which otherwise is not included in the DFT based calculations[16]. For this purpose we have used Grimme's van der Waals dispersion (DFT-D2) correction in all our calculations for the supported semihydrogenated graphene[24,25]. We have checked the validation of the DFT-D2 correction for the case of Ni(111)/graphene interface which is widely studied in comparison with Co(111)/graphene and Cu(111)/graphene interfaces, by comparing our results with previous studies (both experimental and computational) reported in literature.

Table 1. The cell parameters of freestanding semihydrogenated graphene sheet in different H adsorption patterns and transition metal surfaces

Structure	Cell parameter (Å)	
	a	b
Gr	4.27	4.93
UGrH	4.38	5.06
RGrH	4.28	5.09
ZGrH	4.29	5.00
AGrH	4.28	4.85
Ni(111)	4.32	4.98
Co(111)	4.35	5.02
Cu(111)	4.50	5.19

We have obtained the binding energy of graphene on Ni(111) surface (ΔE_{Gr}) to be around –0.17 eV/C atom and the Ni-graphene distance ($d_{Ni\text{-}Gr}$) to be around 2.1 Å, which agrees well with those reported in other computational as well as experimental studies. For example, Gamo *et al.*[27] performed low-energy electron diffraction (LEED) experiments to investigate atomic structure of graphene on Ni(111) surface and found $d_{Ni\text{-}Gr}$ to be around 2.11±0.07 Å that is in excellent agreement with our computed value. Zhao *et al.*[28] obtained $d_{Ni\text{-}Gr}$ around 2.2 Å and ΔE_{Gr} around –0.12 to –0.14 eV using density functional theory calculations with semiempirical van der Waals correction developed by Ortmann *et al.*[29]. Hamada and Otani[30] studied graphene supported on different metal surfaces using van der Waals density functional (vdW-DF)[31] and its second version, vdW-DF2[32], with exchange functional developed by Cooper[33] (C09). Their computed values of ΔE_{Gr} and $d_{Ni\text{-}Gr}$ obtained with vdW-DF C09x (vdW-DF2 C09x) are around –0.18 (–0.14) eV and 2.06 (2.07) Å, which are in good agreement with those reported by our calculations[14]. However when compared with ACDF-RPA results we find that DFT-D2 overestimates the binding energy[16]. Nonetheless the binding distance is in close agreement.

For semihydrogenated graphene supported on TM surface we have determined core-level shifts in the C *1s* states due to the local environment by calculating the core level binding energy (ΔE^C) using the following equation:

$$\Delta E^C = E^{GS} - E^{CFS} \quad (1)$$

where, E^{GS} and E^{CFS} is the ground state and full core-hole final state energy of the system, respectively. ΔE_C is computed for both, hydrogenated and unhydrogenated carbon atoms of graphene. The computed binding energies are then plotted as a Gaussian function, as given by eq. (2), with a width (σ) of 0.5 eV.

$$I(\varepsilon) = \frac{1}{\sigma}\Sigma_{j=1,N_C} \exp\left[\frac{(\varepsilon - \Delta E^C(j))^2}{2\times\sigma^2}\right] \quad (2)$$

where, $I(\varepsilon)$ is intensity at energy ε of the incident X-ray. N_c is the number of carbon atoms whose core level binding energy is calculated. In the pseudopotential based calculations the information regarding the energies of the core states is not available. Therefore the absolute values of computed and experimental binding energies do not match. Hence we have compared the differences in binding energies of hydrogenated and unhydrogenated carbon atoms obtained from our calculation with that obtained from the experimental study. For the calculation of system with corehole we have used full corehole norm-conserving pseudopotential for the excited carbon atom in order to describe the electron-ion interaction. The pseudopotential with a hole in the *1s* core state for C is also taken from the Quantum ESPRESSO website[19]. This pseudopotential had been generated using the Troullier-Martin method[34]. The electronic configuration used for the generation of this pseudopotential is $1s^1\ 2s^2\ 2p^{1.5}$. The kinetic energy cutoff for wavefunction is increased to 65 Ry. The separation between the periodic images of the C atoms with corehole is around 4.38 Å and 5.06 Å along the **a** and **b** directions. On increasing the separation to around 7.59 Å (by using a 3×3 hexagonal cell) the core level shifts change by about 0.1 eV, with respect to the previous case with a smaller separation between the periodic images. We note that these changes are smaller than the differences in the binding energy of the C *1s* electron between the hydrogenated and unhydrogenated C atoms. Therefore all calculations with corehole are performed with the smaller separation between the core-hole atoms.

3. Results and discussion

(I) Determining stable structure of freestanding semihydrogenated graphene

In pristine graphene sheet the unbalanced p_z electrons on every carbon atom form a π-π bonding network. The electronic structure of graphene shows that the occupied bonding and unoccupied anti-bonding states of these p_z electrons cross each other exactly at the Fermi energy. Thus the bandstructure of graphene shows zero bandgap with zero density of states at the Fermi energy[35]. The π-network is however broken locally upon adsorption of H atom. As a result new C-p_z state emerges near Fermi energy which belongs to the carbon atoms that are in close vicinity of the hydrogenated carbon atoms. Šljivančanin *et al.*[2] demonstrated from their first principles study of H dimer on graphite surface that the second H atom adsorbs selectively at a site, neighboring to the first hydrogenation site, with highest local density of states near the Fermi energy. An increase in the local density of states is a consequence of increased charge localization on the carbon atom due to breaking of the π-π bond upon hydrogenation. Therefore the unhydrogenated C

atoms closest to the hydrogenated C will show greater charge localization and hence will be more reactive. Thus we observe that the adsorbed H is present in a closed-packed arrangement rather than in scattered or dispersed patterns on graphene[2-4]. In the present study we make use of this site selectivity of adsorbing H atom to determine the lowest energy structure of the semihydrogenated freestanding graphene. For this purpose we hydrogenate one carbon atom at a time in an orthorhombic unit cell containing 8 C atoms (Fig. 1 (a)). For each hydrogenation step we have determined the charge localization ($\Delta n(r)$) on unhydrogenated C atoms so as to find out the next preferable H adsorption site. The charge localization is determined using the following equation:

$$\Delta n(r) = n^{X}_{\text{H-Gr}}(r) - n^{X\text{-}1}_{\text{H-Gr}}(r) - n_{\text{H}} \qquad (3)$$

In eq. (3), $n^{X}_{\text{H-Gr}}$ is the total charge density of graphene sheet with X number of H adsorbed (*XH-Gr*), $n^{X\text{-}1}_{\text{H-Gr}}$ is the total charge density of graphene sheet with one H atom less than in *XH-Gr* but in the same geometry as *XH-Gr* and *nH* is the charge density of H atom(s) in the same unit cell as that of the hydrogenated graphene sheet. X takes the minimum value of 1 and maximum value of 4, which corresponds to a minimum H coverage of 0.125 ML and a maximum H coverage of 0.5 ML H on graphene sheet respectively. In the beginning hydrogen is adsorbed at C_1, on sublattice α, which gives rise to a non-zero sublattice imbalance. The charge transfer shows that the charge localizes on the neighboring carbon atoms, C_2, C_4 and C_8 of sublattice β as shown in Fig. 1(b). We notice that C_2 and C_8 are equivalent with respect to their local environment and thus they show equal charge localization, which we have confirmed from the exactly same contribution to the density of states (DOS) from these two C atoms near the Fermi energy (in Fig. 1(f)). Therefore hydrogenating either of these two carbon atoms is thermodynamically equivalent. Unlike C_2 and C_8, C_4 has a diagonally opposite hydrogenated carbon atom. So hydrogenating C_4 will form a more denser H cluster than that formed by hydrogenating C_2 or C_8. Hence we find that C_4 shows slightly greater charge localization relative to C_2 and C_8 as shown by the projected DOS in Fig. 1(f). As a consequence hydrogenating C_4 is energetically more favourable (by 0.72 eV) than hydro-

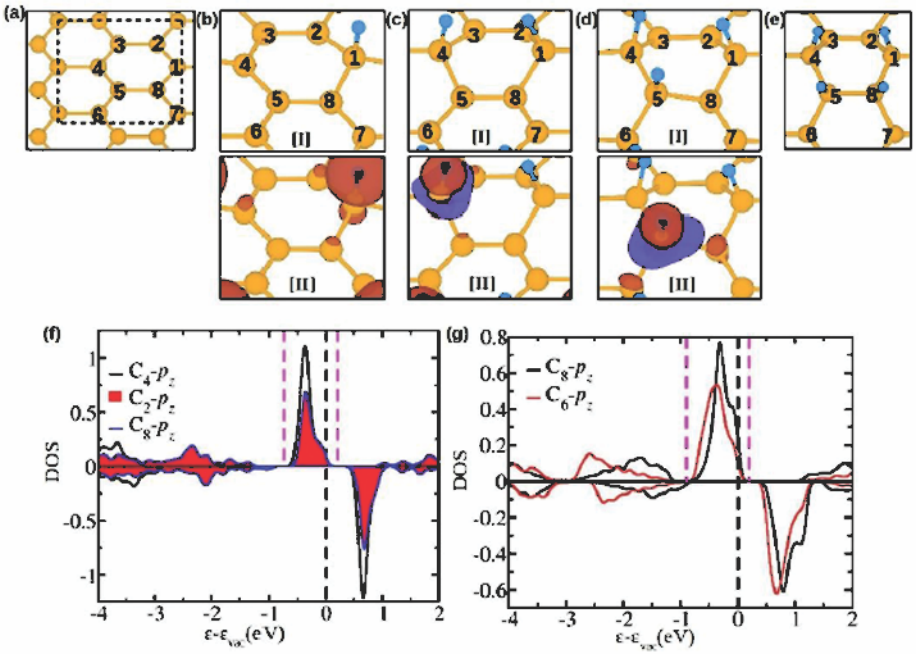

Fig. 1. (a) Structure of freestanding graphene sheet. The black dashed box denotes the orthorhombic unit cell. (b, c, d) Structure (in panel [I]) and charge transfer plot (in panel [II]) for hydrogenated graphene with one, two and three H atoms in the orthorhombic unit cell of graphene, respectively. Charge transfer is determined using eq. (3). The red and blue isosurfaces show accumulation and depletion of charge, respectively. (e) Optimised structure of hydrogenated graphene sheet with four H atoms in the orthorhombic unit cell. (f, g) DOS for C atoms in structures (b) and (d), respectively. In this and the subsequent figures the C and H atoms are denoted by orange and clue colored spheres, respectively.

genating C_2 or C_8. By taking into account the periodic boundary conditions, we find that the structure in Fig. 1(c) is similar to that reported for H trimer on graphene[3]. On adding the second H at C_4 the chemical imbalance within the graphene lattice is nullified. With H adsorbed at C_1 the second H adsorbed on C_4 give rise to charge localization on C_3 and C_5 (Fig. 1(c) [II]). C_3 and C_5 are equivalent with respect to their local environment and hence hydrogenating either of them amounts to equal thermodynamic stability. So we add the third H in the unit cell at C_5 and we find that the charge localizes on C_6 and C_8, as shown in Fig. 1(d) [II]. C_8 has two neighboring hydrogenated C while C_6 has only one. Therefore similar to the case of adsorption of the second H atom we find that hydrogenating C_8 is more favorable (by around 0.80 eV) because it forms a more compact H cluster on the graphene sheet than that formed upon hydrogenating C_6. Consistently we find from the DOS of $C_{6,8}$-2*p* that the charge accumulation is greater on C_8 than that on C_6 (Fig. 1(g)). Thus we add the fourth and the last H on C_8. We do not add any more H atoms as we are only interested in studying the hydrogenation of graphene at 0.5 ML H coverage.

An important observation to note here is that every new H atom that is added in the cell is adsorbed on a different sublattice than in the previous step. This shows that the chemical imbalance majorly governs the site selective adsorption of H on graphene. The charge redistribution guides us to the lowest energy structure of semihydrogenated graphene which is shown in Fig. 1(e). The hydrogenation pattern in this lowest energy structure form strips of hydrogen atoms along the armchair direction of the graphene sheet. Therefore we call this structure as armchair graphone (AGrH) consistent with other nomenclature like rectangular graphone (RGrH)[5] and zigzag graphone (ZGrH)[6]. Further we have compared the stability of AGrH with the other three earlier reported semihydrogenated graphene structures (GrH, RGrH and ZGrH) by determining the binding energy of H, ΔE_H, using the following equation:

$$\Delta E_H = \frac{(E_{Gr/H} - E_{Gr} - 4\times E_H)}{A} \qquad (4)$$

The first ($E_{Gr/H}$) and second (E_{Gr}) terms on the right hand side (RHS) of eq. (4) are the total energies of hydrogenated and pristine graphene sheet in freestanding condition, respectively. The third term (E_H) is the total energy of an isolated H atom. *A* is the unit cell area of the hydrogenated graphene sheet. We find that the hydrogen atoms bind strongest on graphene sheet in AGrH with ΔE_H of around –0.30 eV/Å^2. In RGrH and Z-GrH ΔE_H is around –0.28 eV/Å^2 and that in UGrH is around –0.12 eV/Å^2. We have shown the optimized structures of all the four semihydrogenated graphene sheets in Fig. 2. A more detailed comparison of the stability and properties of freestanding semihydrogenated graphene in the four H adsorption patterns are included in the supported information.

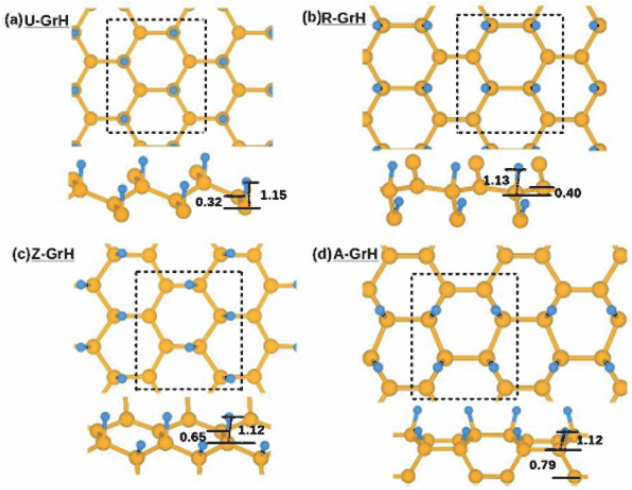

Fig. 2. (a)-(d) Side and top-view geometry of the uniform, rectangular, zigzag and armchair hydrogen patterns on the graphene sheet, respectively. The black dotted box is the orthorhombic cell containing 8 C atoms. The distances displayed in the figures are in angstrom units.

(II) Semihydrogenated graphene supported on TM surface

(A) Structure and electronic properties:

We have next studied semihydrogenation of graphene sheet supported on three transition metal surfaces, namely Ni(111) and Co(111) surfaces, on which the epitaxial graphene sheet is found to be chemisorbed and Cu(111) surface which physisorbs the epitaxial graphene sheet. From Ni(111) to Co(111) to Cu(111) surfaces the strain on the epitaxial graphene increases as 1.2%, 2.0% and 5.7%, respectively. By comparing the lattice parameters of semihydrogenated graphene in different H adsorption patterns and the three TM surfaces we find that the strain on semihydrogenated graphene remains trifling when supported on Ni(111) and Co(111) surfaces while it is significant when on Cu(111) sur-

face. The lattice parameters of the four freestanding semihydrogenated graphene and the three transition metal surfaces are given in Table 1. On Ni(111) surface we find that all four H patterns are equally stable with binding energy of H (ΔE_H^{supp}) around –0.39 eV/Å^2. On Co(111) surface AGrH and ZGrH are equally stable with ΔE_H^{supp} of around –0.37 eV/Å^2. RGrH on Co(111) is slightly more stable with ΔE_H^{supp} around –0.38 eV/Å^2 while UGrH shows less stability with ΔE_H^{supp} around –0.36 eV/Å^2. Similarly on Cu(111) surface AGrH and ZGrH again show equal stability (ΔE_H^{supp} = –0.34 eV/Å^2); RGrH is most stable (ΔE_H^{supp} around –0.37 eV/Å^2) and UGrH is least stable (ΔE_H^{supp} = –0.33 eV/Å^2). ΔE_H^{supp} is determined using an equation analogous to that of eq. (4) where $E_{Gr/H}$ and E_{Gr} on the RHS are replaced with total energies of semihydrogenated graphene ($E_{TM/Gr/H}$) and pristine graphene ($E_{TM/Gr}$) on TM surface, respectively. Even though the stability of all four structures on Ni(111) surface are equal the sites occupied by the C atoms in each structure are different. Similarly different configurations of semihydrogenated graphene for different H adsorption patterns are observed on Co(111) and Cu(111) surfaces. The top and side view of the relaxed structures of the semihydrogenated graphene on Ni(111), Co(111) and Cu(111) are shown in Figs. 3, 4 and 5, respectively. The UGrH on all three TM surfaces takes the top-fcc configuration in which the hydrogenated (unhydrogenated) C is at the fcc (top) site. This is consistent with our earlier study on uniform graphone supported on Ni(111) and Co(111)[14,15]. Next RGrH takes the bridge-top configuration on all the three TM surfaces. The bridge-top configuration is formed when one C is at the bridge between fcc and top sites while the other one is at the bridge between hcp and top sites. Thus the C-C bonds lie above the surface TM atom. Bridge-top configuration is found to be equally stable to top-fcc configuration for clean graphene sheet on Ni(111)[28]. In RGrH the C-C bond over the top-site is between the same kind of carbon atoms, i.e. both are either unhydrogenated or hydrogenated. Next, ZGrH on Ni(111) surface takes the bridge-top configuration such that the C-C bond over the top-site is between one unhydrogenated C and one hydrogenated C. A different structure is obtained for ZGrH on Co(111) and Cu(111) where the carbon atoms are laterally shifted by 0.4–0.5 Å from the top sites and 0.3–0.4 Å from fcc sites. Hence we have named the configuration as

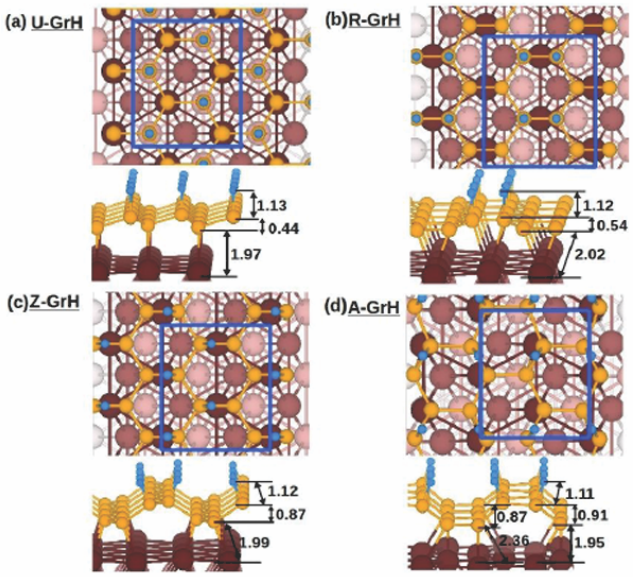

Fig. 3. Topview (in top panel) and side-view (in bottom panel) of configurations of uniformly hydrogenated graphone (UGrH) (a), rectangular graphone (RGrH) (b), zigzag graphone (c) and armchair graphone (d) on Ni(111) surface. In top-view the bigger dark (brown) colored atoms are surface Ni atoms and lighter ones are the Ni atoms that resides below the surface. The blue rectangular box denotes the unit cell. The distances shown in side-view figures are in angstrom units.

shifted-top-fcc configuration. AGrH on Co(111) takes bridge-top configuration while on Ni(111) and Cu(111) the C atoms are present in shifted-top-fcc configuration. The lateral shift in the C atoms with respect to Ni (Cu) atoms at the top-sites is around 0.3 (0.3–0.4) Å while at fcc-sites is around 0.3–0.4 (0.5–0.6) Å in AGrH on Ni(111) (Cu(111)) surface.

At this point few questions arise: (a) First question is how is it that on Ni(111) surface alone all the hydrogenation patterns on the semihydrogenated graphene, including UGrH, are equally stable? (b) Next question is why are the four semihydrogenated graphene structures present in different configurations on the TM surfaces? (c) Further among the four stable patterns only UGrH structure on Ni(111) surface was recognised experimentally using XPS measurements. Why were there no signatures of other H adsorption pattern in the XPS studies[13].? To answer the first question we have decomposed the ΔE_H^{supp} into its constituent energy terms, in the following equations. The competing energy terms are (1) interaction energy (E^{int}) which is the sum of C-H interaction

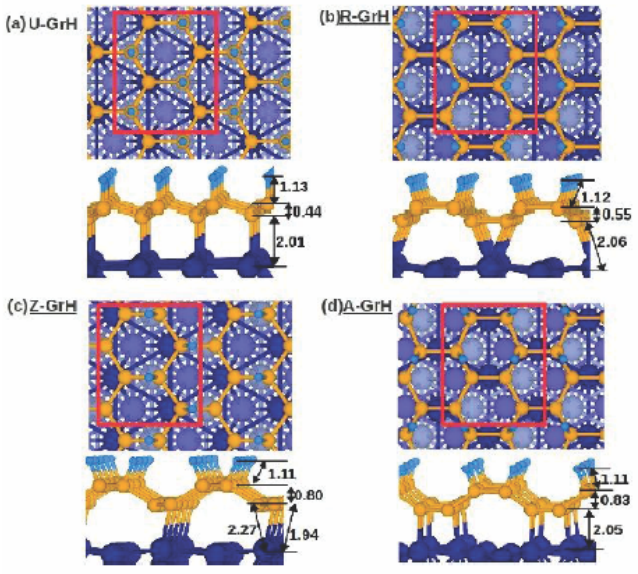

Fig. 4. Topveiw (in top panel) and side-view (in bottom panel) of configurations of uniformly hydrogenated graphone (UGrH) (a), rectangular graphone (R-GrH) (b), zigzag graphone (Z-GrH) and (c) armchair graphone (A-GrH) (d) on Co(111). In top-view the bigger dark (blue) colored atoms are surface Co atoms and lighter ones are the Co atoms that reside below the surface. The red rectangular box denotes the unit cell. The distances shown in side-view figures are in Å.

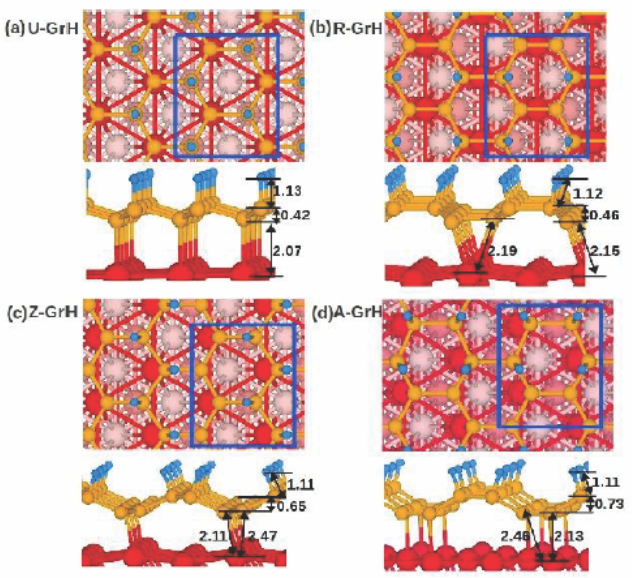

Fig. 5. Topveiw (in top panel) and side-view (in bottom panel) of configurations of uniformly hydrogenated graphone (UGrH) (a), rectangular graphone (R-GrH) (b), zigzag graphone (Z-GrH) (c) and armchair graphone (A-GrH) (d) on Cu(111). In top-view the bigger dark (red) colored atoms are surface Co atoms and lighter ones are the Cu atoms that reside below the surface. The blue rectangular box denotes the unit cell. The distances shown in side-view figures are in angstrom units.

energy $\left(E^{\text{int}}_{\text{Gr-H}}\right)$ and H-H interaction energy $\left(E^{\text{int}}_{\text{H-H}}\right)$ and (2) strain energy $\left(E^{\text{strain}}_{\text{Gr}}\right)$.

$$\Delta E^{\text{supp}}_{\text{H}} = \left[E^{\text{int}}_{\text{Gr-H}} + E^{\text{int}}_{\text{H-H}}\right] + E^{\text{strain}}_{\text{Gr}} \quad (5)$$

$\left(E^{\text{int}}_{\text{Gr-H}}\right)$, first term in the RHS of eq. (5) is given by,

$$E^{\text{int}}_{\text{Gr-H}} = \frac{E_{\text{TM/Gr/H}} - E'_{\text{TM/Gr}} - E'_{4\text{H}}}{A} \quad (6)$$

where, $E_{\text{TM/Gr/H}}$ is the total energy of the combined system. The second (third) term in eq. (6), $E'_{\text{TM/Gr}}$ ($E'_{4\text{H}}$), is the total energy of graphene on TM surface (H atoms) obtained by removing the H (graphene and TM substrate) atoms from the optimised geometry of the combined system. $\left(E^{\text{int}}_{\text{H-H}}\right)$ is the second term in eq. (5) which is evaluated with the following equation.

$$E^{int}_{HH} = \frac{E'_{4H} - 4\times E_H}{A} \quad (7)$$

$E'_{4\text{H}}$ is same as defined in eq. (6) and E_{H} is the energy of a single isolated H atom. The last term in eq. (5) $\left(E^{\text{strain}}_{\text{Gr}}\right)$ corresponds to the strain arising in epitaxial graphene on TM surface due to change in its geometry upon hydrogenation. It is determined by the difference between the energy of graphene on TM surface when present in the same geometry as in the combined system ($E'_{\text{TM/Gr}}$) and total energy of completely relaxed pristine graphene on TM surface ($E_{\text{TM/Gr}}$), as given below in eq. (8):

$$E^{\text{strain}}_{\text{Gr}} = \frac{E'_{\text{TM/Gr}} - E_{\text{TM/Gr}}}{A} \quad (8)$$

Fig. 6 shows bar plot of $\Delta E^{\text{supp}}_{\text{H}}$ for different semihydrogenated structures on the three TM surfaces along with the contribution of the two competing energy terms. We note that E^{int} is highly dominating over $E^{\text{strain}}_{\text{Gr}}$ and thus semihydrogenated graphene is stable on all three TM surfaces. On Ni(111) surface both E^{int} and $E^{\text{strain}}_{\text{Gr}}$ shows the following trend among the four semihydrogenated structures:

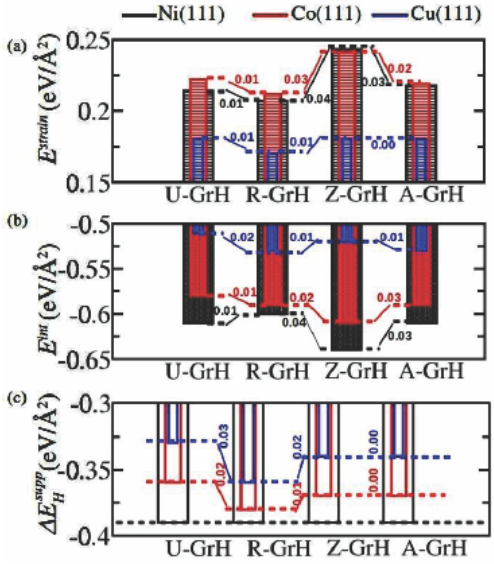

Fig. 6. (a) Strain energy, (b) interaction energy and (c) binding energy of H on graphene supported on Ni(111) (black), Co(111) (red) and Cu(111) (blue) surfaces.

ZGrH > UGrH = AGrH > RGrH. Moreover we note that the difference in the net energy gain by the system (i.e. change in E^{int}) is compensated exactly by the difference in the energy cost by the system (change in E_{Gr}^{strain}) as we move from one structure to other on Ni(111) surface, thereby making all the patterns equally favorable. On Co(111) as well as on Cu(111) surfaces the trends observed for E_{Gr}^{strain} are different from that for E^{int}. On Co(111) surface trends in E^{int} and $\left(E_{Gr}^{strain}\right)$ are ZGrH > RGrH = AGrH > UGrH and ZGrH > AGrH = UGrH > RGrH, respectively. ZGrH on Co(111) surface shows largest E^{int} (–0.61 eV/Å^2) while UGrH has the least (–0.58 eV/Å^2). RGrH and AGrH has equal E^{int} (–0.59 eV/Å^2) which is less than that in ZGrH. Though ZGrH on Co(111) surface has largest E^{int} but it also has largest E_{Gr}^{strain} (0.24 eV/Å^2) resulting in –0.37 eV/Å^2 of ΔE_H^{supp} which equal to that in AGrH on Co(111). Both UGrH and AGrH on Co(111) shows 0.02 eV/Å^2 smaller E_{Gr}^{strain} than ZGrH on Co(111) surface. But since E^{int} in UGrH is less than that in AGrH on Co(111) by about 0.01 eV/Å^2 the resultant ΔE_H^{supp} is larger in AGrH (–0.37 eV/Å^2) than in UGrH (–0.36 eV/Å^2) on Co(111) surface. The least E_{Gr}^{strain} is observed in RGrH (0.21 eV/Å^2) resulting in largest ΔE_H^{supp} of about –0.38 eV/Å^2. On Cu(111) we find the trend in E^{int} as RGrH = AGrH > ZGrH > UGrH and that in E_{Gr}^{strain} as UGrH = ZGrH = AGrH > RGrH. RGrH shows largest E^{int} (–0.53 eV/Å^2) and smallest E_{Gr}^{strain} (0.17 eV/Å^2) which makes it the most stable structure. The remaining three structures show equal strain of around 0.18 eV/Å^2. Thus their relative stability is decided by E^{int}. AGrH has equal E^{int} as in RGrH on Cu(111) thus it has second largest ΔE_H^{supp} around –0.35 eV/Å^2. E^{int} in ZGrH and UGrH is around –0.52 eV/Å^2 and –0.51 eV/Å^2 which results in ΔE_H^{supp} of around –0.34 eV/Å^2 and –0.33 eV/Å^2, respectively.

For addressing the second question we have evaluated interaction energy between TM surface and epitaxial graphene sheet when it is clean and when it is semihydrogenated in different H adsorption patterns. The TM-Gr interaction energy $\left(E_{TM\text{-}Gr}^{int}\right)$ is determined using eq. (10)

$$E_{TM\text{-}Gr}^{int} = \frac{E'_{TM/Gr/H} - E'_{TM} - E'_{Gr/H}}{A} \qquad (9)$$

where, the terms in the RHS are the total energies of semihydrogenated graphene on TM surface, the clean TM surface and the freestanding semihydrogenated graphene sheet, all calculated using their respective geometries as in the semihydrogenated graphene supported on TM surfaces. For the system of clean graphene on TM surface the first and third term in eq. (10) are replaced with total energy of clean graphene on TM surface and total energy of freestanding graphene. $E_{TM\text{-}Gr}^{int}$ for different systems are listed in Table 2. As freestanding UGrH (AGrH) is highly unstable (stable) we find that $E_{TM\text{-}Gr}^{int}$ is stronger (weaker) for UGrH (AGrH) on all three TM surface. ΔE_H^{supp} has direct dependence on $E_{TM\text{-}Gr}^{int}$ which is shown in eq. (11).

$$\Delta E_H^{supp} = \frac{\left[E_{TM\text{-}Gr}^{int} + \Delta E'_H - E'^{int}_{TM\text{-}Gr}\right] + E_{Gr}^{strain} + E_{H\text{-}H}^{int}}{A} \qquad (10)$$

Table 2. Interaction energy of graphene (column 2) and semihydrogenated graphene in different H adsorption patterns (columns 3–6) with its transition metal substrates in eV/Å^2

Substrate	Gr	UGrH	RGrH	ZGrH	AGrH
Ni(111)	–0.06	–0.34	–0.20	–0.22	–0.19
Co(111)	–0.08	–0.32	–0.20	–0.19	–0.17
Cu(111)	–0.03	–0.21	–0.11	–0.09	–0.09

$\Delta E'_{H}$ and $E^{int}_{TM\text{-}Gr}$ are binding energy of H in freestanding semihydrogenated graphene when it has the same geometry as on TM surface and interaction energy of clean graphene sheet and TM surface when the system of epitaxial graphene on TM surface is in the same geometry as when semihydrogenated. The rest of the terms are defined earlier in this paper (E^{strain}_{Gr} in eq. (8) and $E^{int}_{H\text{-}H}$ in eq. (7)). Note that the first three terms in eq. (11), included within square brackets, amounts to $E^{int}_{Gr\text{-}H}$ which is defined in eq. (6). Thus stronger $E^{int}_{TM\text{-}Gr}$ stronger is $E^{int}_{Gr\text{-}H}$ and more is the stability of semihydrogenated structure (or larger ΔE^{supp}_{H}). Hence the direct dependence of stability of semihydrogenated graphene on TM surface on $E^{int}_{TM\text{-}Gr}$ suggests that the role of substrate is to stabilise the unhydro-genated C. The C-H interaction energy in freestanding semihydrogenated graphene is given in Fig. 1 of the Supporting information which is weaker than that when the semihydrogenated graphene sheet is supported on TM surfaces. In order to achieve maximum stability of the unhydrogenated C the semihydrogenated graphene sheet chooses different configurations on the TM surfaces. Thus the semihydrogenated graphene with uniform H pattern stabilises in top-fcc configuration even when we start with bridge-top configuration on Ni(111) surface. Similarly ZGrH and AGrH on Ni(111) moves to bridge-top and shifted-top-fcc configuration from the initial top-fcc configuration. We were able to optimise AGrH on Ni(111) in bridge-top configuration however, it shows higher total energy than shifted-top-fcc configuration by 108 meV. RGrH also chooses bridge-top configuration over top-fcc configuration by about 72 meV of energy. In the same manner we obtain different configurations of different semihydrogenated graphene sheet on Co(111) and Cu(111) surfaces. We further note that unlike UGrH and RGrH structures, AGrH and ZGrH structures does not show same configuration as we change the underlying substrate. For explaining this observation we have calculated strain energy in the semihydrogenated graphene sheet when it is freestanding but in the same geometry as it is on the TM surfaces. The strain energy is calculated by taking the difference between total energies of freestanding semihydrogenated graphene when it is in the same geometry as on TM surface and when it is completely relaxed. We find that for both, UGrH and RGrH, the strain energy remains more or less constant on all three TM surfaces to 0.03 eV/Å^2 and 0.04 eV/Å^2, respectively. Therefore for these two H patterns we do not observe change in their configurations with different metal substrates. For ZGrH the strain energy on Co(111) and Cu(111) surfaces are equal and around 0.03 eV/Å^2 while it is higher on Ni(111) surface which is around 0.05 eV/Å^2. Thus on Co(111) and Cu(111) surfaces ZGrH chooses same configuration (shifted-top-fcc) while on Ni(111) surface it settles in a different configuration (bridge-top). Similarly for AGrH strain energy is higher when placed on Ni(111) surface (0.04 eV/Å^2) and Cu(111) surface (0.05 eV/Å^2) than when placed on Co(111) surface (0.02 eV/Å^2). Therefore on Ni(111) and Cu(111) surfaces AGrH is present in shifted-top-fcc configuration while on Co(111) surface it is present in bridge-top configuration.

In order to address the last question we have computationally determined the core-level shifts for C *1s* of unhydrogenated and hydrogenated C in all the Ni(111) surface-supported structures and have compared with the experimental C *1s* spectra reported by Zhao *et al.*[13] for semihydrogenated graphene on Ni(111) surface. In Fig. 7

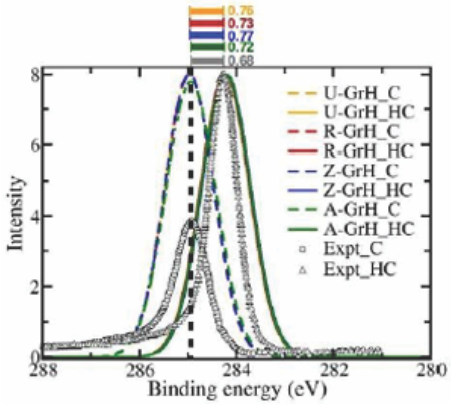

Fig. 7. Corelevel shifts of C *1s* of the unhydrogenated carbon (C) and hydrogenated carbon (HC) in the semihydrogenated graphene sheet supported on Ni(111) surface. The dotted and solid curves corresponds to C and HC, respectively. The peaks are shifted with respect to the experimental peak of the unhydrogenated C atom at 284.96 eV. The experimental data is obtained from the XPS studies performed by Zhao *et al.*[13]. The difference in the binding energy are noted above the plot.

we have shown the C *1s* spectra of hydrogenated and unhydrogenated carbon atoms with dashed and continuous lines, respectively. The plots for all the four structures are shifted so as to align the peaks corresponding to the unhydrogenated carbon atoms obtained from our study with the peak for unhydrogenated carbon atoms obtained from the experimental measurement at 284.96 eV by Zhao *et al.*[13]. The spectra obtained for all the four structures from our calculations match quite well with the experimental one. The area under the peaks corresponding to the unhydrogenated carbon atom and hydrogenated carbon atom are equal implying that the hydrogen coverage is 0.5 ML. Also the spectra for all four Ni(111)/HGr structures closely follow each other which is consistent with our result that the four semihydrogenated structures on Ni(111) surface are equally favourable. The small differences in the corelevel shifts (0.01–0.05 eV) due to change in the H adsorption patterns of the semihydrogenated graphene are quite smaller than the experimental resolution (0.2 eV) and hence probably are not detected. Similar corelevel shifts were determined for structures on Co(111) and Cu(111) surfaces. However since XPS studies on semihydrogenated graphene supported on Co(111) and Cu(111) surfaces has not been reported we are unable to make any comparisons of our results on these surfaces with those from experiments. The corresponding corelevel shift plots of semihydrogenated graphene on Co(111) and Cu(111) are shown in Figs. 4(a) and 4(b) of the Supporting information. Where for the Ni surface we find that CLS vary between 0.72–0.77 eV, for Co(111) they vary between 0.7 to 0.85 eV and for Cu(111) they vary between 0.96 to 1.15 eV. Thus again it will be difficult to discern different H adsorption patterns on Co(111) as well as Cu(111) surfaces if the resolution is set to 0.2 eV in the XPS measurements. Though not discernible from XPS measurements our study shows that each structure displays different interfacial electronic and magnetic properties. From Figs. 3, 4 and 5 we observe variation in the TM-C bondlength suggesting variation in TM-C interaction (which is calculated above) among different structures. This variation in TM-C interaction in turn results in variation of magnetic moments on surface TM and graphene sheet. In Figs. 8 and 9 we have plotted the average magnetic moment on surface TM and graphene sheet for the four semihydrogenated structures supported on TM surfaces, respectively. Weaker (stronger) is the TM-C bondlength larger is the magnetic moment on surface TM (C) atoms. In UGrH on Ni(111) surface the Ni-C bond length is around 1.96 Å which slightly increases to 1.99 Å in ZGrH. As a consequence the magnetic moment on surface Ni in UGrH on Ni(111) surface is around 0.16 μ_B which is less compared to 0.26 μ_B in ZGrH on Ni(111) surface. In case of AGrH on Ni(111) surface there are two kind of Ni-C bondlengths: (i) one where the unhydrogenated C is in shifted top site and the Ni-C bond length is stronger of around 1.94 Å and (ii) the other where the unhydrogenated C is in the shifted fcc site with weaker Ni-C bond length of around 2.15 Å. Thus the stronger of the two interactions result in 0.26 μ_B while the weaker results in 0.40 μ_B magnetic moment on the surface Ni. Finally in RGrH only half of the Ni atoms interact with pairs of unhydrogenated C (Ni-C bondlength = 2.03 Å) while the other half has pairs of hydrogenated C above them. Therefore, those Ni atoms interacting with unhydrogenated C have quenched magnetic moment of 0.42 μ_B while the rest of the Ni atoms have a magnetic moment of 0.64 μ_B that is closely comparable in magnitude with what is observed for the clean Ni(111) surface (0.71 μ_B). The interaction with surface Ni atoms induces magnetic moment on unhydrogenated C of the graphene sheet giving rise to small net magnetic moment which is an order of magnitude smaller than that of surface Ni atom as shown in Fig. 8. On Co(111) surface UGrH again shows stronger Co-Gr interaction which results in quenched magnetic moment on surface Co of around 1.30 μ_B with respect to 1.78 μ_B in clean Co(111) surface. In shifted-top-fcc configuration of ZGrH structure we find that only half of the surface Co interacts with the unhydrogenated C resulting in Co-C

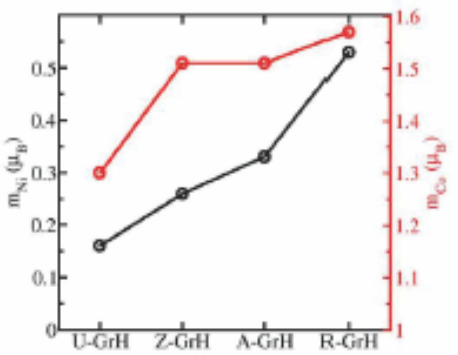

Fig. 8. Net magnetic moment of surface Ni and Co atoms in four semihydrogenated structures.

bondlength of around 1.94 Å. Therefore half of the surface Co show quenched magnetic moment of around 1.15 μ_B while the remaining Co show larger magnetic moment of around 1.87 μ_B. Thus the net magnetic moment of surface Co in ZGrH on Co(111) is around 1.51 μ_B. Like on Ni(111) surface, RGrH on Co(111) is present in bridge-top configuration such that half of the surface Co atoms interact with the pair of unhydrogenated C making Co-C bondlength of around 2.07 Å. Thus half of the surface Co have quenched magnetic moment (1.32 μ_B) while the remaining half have larger magnetic moment (1.82 μ_B) making the net magnetic moment on surface Co to be around 1.57 μ_B. Similar to RGrH, AGrH on Co(111) is present in bridge-top configuration with only half Co atoms interacting with the pair of unhydrogenated C (Co-C bondlength = 2.05 Å) which results in quenched magnetic moment on surface Co of around 1.18 μ_B. The remaining half surface Co have magnetic moment of around 1.84 μ_B which results in the net magnetic moment on surface Co of around 1.51 μ_B. As in the case on Ni(111) we find weak net magnetic moment on graphene when the semihydrogenated graphene sheets are supported on Co(111). However on Co(111) surface the induced moment on graphene is larger than on Ni(111) as also seen from Fig. 9.

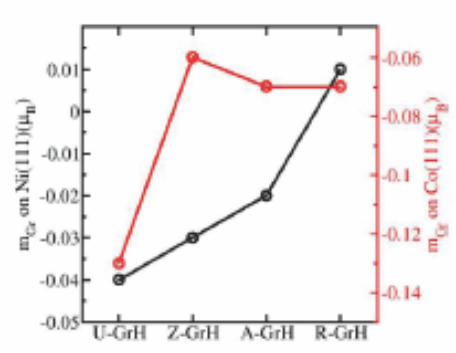

Fig. 9. Net magnetic moment on graphene sheet in four semihydrogenated structures supported on Ni(111) (black) and Co(111) (red) surfaces.

Unlike Ni and Co surfaces, Cu(111) is non-magnetic. Hence the three non-magnetic semihydrogenated graphene structures, namely AGrH, ZGrH and RGrH remains non-magnetic on Cu(111) while the ferromagnetic structure, UGrH show magnetic moment of around 0.22 μ_B on each unhydrogenated C in the graphene sheet. The surface Cu atoms in UGrH on Cu(111) also show weak magnetic moment of around 0.08 μ_B.

Further, we have studied the contribution to the DOS from atoms at the interface of semihydrogenated graphene and TM surfaces. In Fig. 10 we have shown the DOS projected on the *d*-orbitals of the surface TM and on both hydrogenated and unhydrogenated C for all the four structures. We notice that the supported semihydrogenated graphene in all four H adsorption patterns show non-zero DOS at Fermi level, which arise primarily from the interaction of unhydrogenated C atoms with the TM substrate. The interaction at the interface causes variation in the density of states of surface TM atoms with H adsorption patterns. We have quantified this variation by calculating spin polarization (S) of TM-*d* using eq. (9).

$$S = \frac{D^{\uparrow}(\varepsilon_F) - D^{\downarrow}(\varepsilon_F)}{D^{\uparrow}(\varepsilon_F) + D^{\downarrow}(\varepsilon_F)} \times 100 \qquad (11)$$

where, $D^{\uparrow/\downarrow}(\varepsilon_F)$ is the density of state of spin up/down at the Fermi energy. The positive (negative) *S* suggests that there is density of states from spin up (down) electrons. The spin polarization of Ni-*d* in UGrH, RGrH and AGrH are 67.7%, 78.8% and 56.4%, respectively while that in ZGrH is only 9.9%, where we notice both the spin channels heavily contribute in conduction. The interaction with Ni(111) induces smaller spin polarization, relative to that in Ni-*d*, in semihydrogenated graphene sheet which are around 6.3%, 7.8%, –2.5% and 19.7% for UGrH, RGrH, ZGrH and AGrH, respectively. Similarly spin polarization of Co-*d* in UGrH (–68.8%), RGrH (–79.5%), ZGrH (–78.4%) and AGrH (–71.2%) induces spin polarization in the semihydrogenated graphene which are around 31.1%, 24.6%, 4.8% and 29.2%. The spin polarization of semihydrogenated graphene supported on Co(111) are greater than that of those supported on Ni(111) surface. However the spin polarization in Co-*d* and graphene have opposite sign. Thus interfaces with Ni(111) and Co(111) surfaces with different semihydrogenated graphene structures will give rise to weak or non spin polarized conduction. On Cu(111) structure with uniform hydrogen pattern show spin polarization of Cu-*d* (–60.2%) and semihydrogenated graphene sheet (–61.1%) suggesting much higher possibility of spin polarised conduction than in structures on Ni(111) and Co(111) surfaces. The states of

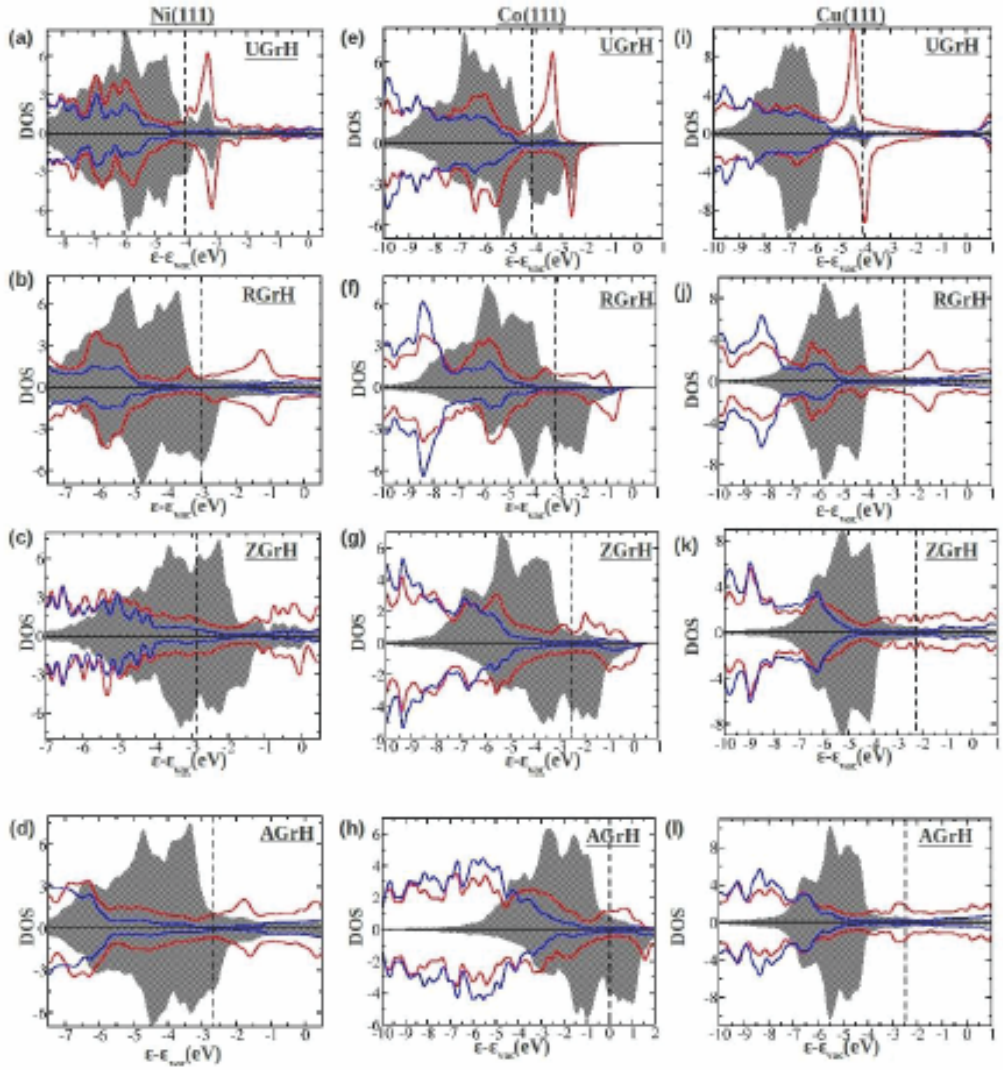

Fig. 10. Projected DOS of surface TM atom (shaded grey), unhydrogenated C (red) and hydrogenated C (blue) in (a, e, i) UGrH, (b, f, j) RGrH, (c, g, k) ZGrH and (d, h, l) AGrH supported on TM(111) surface. The energies are shifted with respect to vacuum energy. The vertical dashed line denotes Fermi energy.

the interfacial atoms at remaining three structures on Cu(111) are non-spin-polarised.

4. Conclusions

We have carried out detailed investigations of semihydrogenated graphene sheet when freestanding and when supported on a (111) surfaces of Ni, Co and Cu. Our calculations suggest that the preferred H adsorption pattern on free standing graphene is determined by two factors: (a) minimization of sublattice imbalance and (b) packing of the H atoms. Based on these two factors we have identified the armchair graphone as the most stable configuration for the semihydrogenated freestanding graphene. Further, upon semihydrogenating the graphene sheet on a Ni(111) support alone we find that all the different adsorption patterns are equally favorable. The reason for this is attributed to the fact that the energy gained is balanced equally with energy loss as we move from one structure to other which is observed neither on Co(111) surface nor on Cu(111) surface. Further importantly we note from core-level shifts in semihydrogenated graphene supported on (111) surface of Ni, Co and Cu that the four H adsorption patterns can be distinguished

in XPS measurements if and only if the resolution less than 0.2 eV. For structures on Ni(111), Co(111) and Cu(111) surface the required minimum resolution is around 0.05 eV, 0.1 eV and 0.19 eV so that at least two structures are discerned. However such small resolution is extremely difficult in current setup for XPS measurements. We further investigated interfacial properties at different structures on the three TM surfaces. We find that though the stability of different semihydrogenated graphene structures are similar they show varied structural, electronic and magnetic properties. The interface with the ferromagnetic Ni(111) and Co(111) surfaces induces small magnetic moment in the non-magnetic semihydrogenated graphene structure, namely RGrH, ZGrH and AGrH. However magnetic moment in ferromagnetic UGrH is highly quenched. On Cu(111) surface RGrH, ZGrH and AGrH retain their non-magnetic behaviour while UGrH show larger magnetic moment that observed on Ni(111) and Co(111) surfaces. Furthermore we find the magnetic moment on surface Ni and Co atoms are quenched with stronger interaction with unhydrogenated C in semihydrogenated graphene. The TM-C interaction in UGrH on Cu(111) surface induces small magnetic moment on surface Cu atoms. Moreover, this interface, of UGrH and Cu(111) surface show high possibility for spin polarised conduction than any other interface studied in this paper. Hence in our opinion to realistically model these interfaces and throw light on their properties, it is important to consider all the H adsorption patterns reported in this work.

Acknowledgements

The authors would like to acknowledge CDAC, Pune, India and Center for Modeling and Simulation, University of Pune, India for providing computational facility. NJ would like to acknowledge IISER Pune for scholarship. PG would like to acknowledge DST-Nanomission, India grants no. SR/NM/NS-1285/2014 and SR/NM/NS-15/2011 for funding.

Supporting Information

The supporting information contains: (1) electronic and magnetic properties of different semihydrogenated graphene sheet in freestanding condition, (2) figure showing C-H interaction in different freestanding semihydroegnated graphene and (3) core-level shifts of different semihydrogenated graphene structures on Co(111) and Cu(111) surfaces.

References

1. J. Zhou, Q. Wang, Q. Sun, X. Chen, Y. Kawazoe and P. Jena, *Nano Lett.*, 2009, **9**, 3867.
2. Ž. Šljivančanin, E. Rauls, L. Hornekær, W. Xu, F. Besenbacher and B. Hammer, *J. Chem. Phys.*, 2009, **131**, 084706.
3. Ž. Šljivančanin, M. Andersen, L. Hornekær and B. Hammer, *Phys. Rev. B*, 2011, **83**, 205426.
4. R. Balog, B. Jørgensen, J. Wells, E. Lægsgaard, P. Hofmann, F. Besenbacher and L. Hornekær, *J. Am. Chem. Soc.*, 2009, **131**, 8744.
5. L. Feng and W. Zhang, *AIP Advances*, 2012, **2**, 042138.
6. Ž. Šljivančanin, R. Balog and L. Hornekær, *Chem. Phys. Lett.*, 2012, **541**, 70.
7. P. Khomyakov, G. Giovannetti, P. Rusu, G. Brocks, J. van den Brink and P. Kelly, *Phys. Rev. B*, 2009, **79**, 195425.
8. A. Preobrajenski, M. Ng, A. Vinogradov and N. Mårtesson, *Phys. Rev. B*, 2008, **78**, 073401.
9. S. Kozlov, F. Viñes and A. Görling, *J. Phys. Chem. C*, 2012, **116**, 7360.
10. L. Khyl, R. Balog, T. Angot, L. Hornekær and R. Bisson, *Phys. Rev. B*, 2016, **93**, 115403.
11. S. Son, C. Holroyd, J. Clough, A. Horn, S. Kochler and C. Casiraghi, *Appl. Phys. Lett.*, 2016, **109**, 243103.
12. M. Ng, R. Balog, L. Hornekær, A. Preobrajenski, N. Vinogradov, N. Mårtesson and K. Schulte, *J. Phys. Chem. C*, 2010, **114**, 18559.
13. W. Zhao, J. Gebhardt, F. Späth, K. Gotterbam, C. Gleichweit, H. Steinrück, A. Görling and C. Papp, *Chem. Eur. J.*, 2015, **21**, 3347.
14. N. Joshi, N. Ballav and P. Ghosh, *Phys. Rev. B*, 2012, **86**, 121411(R).
15. N. Joshi, I. Kaul, Nirmalya Ballav and P. Ghosh, *AIP Conf. Proc.*, 2013, **1512**, 694.
16. T. Olsen and K. Thygesen, *Phys. Rev. B*, 2013, **87**, 075111.
17. P. Giannozzi, S. Baroni, N. Bonini, M. Calandra, R. Car, C. Cavazzoni, D. Ceresoli, G. Chiarotti, M. Cococcioni, I. Dabo, A. Dal Corso, S. de Gironcoli, S. Fabris, G. Fratesi, R. Gebauer, U. Gerstmann, C. Gougoussis, A. Kokalj, M. Lazzeri, L. Martin-Samos, N. Marzari, F. Mauri, R. Mazzarello, S. Paolini, A. Pasquarello, L. Paulatto, C. Sbraccia, S. Scandolo, G. Sclauzero, A. Seitsonen, A. Smogunov, P. Umari and R. Wentzcovitch, *J. Phys. Condens. Matter, 2009,* **21**, 395502.
18. D. Vanderbilt, *Phys. Rev. B*, 1990, **41**, 7892.
19. Pseudopotentials for C (C.pbe-rrkjus.UPF), C with 1s core-hole (C.star1s-pbe-mt_gipaw.UPF), Ni (Ni.pbe-nd-rrkjus. UPF) and H (H.pbe-rrkjus.UPF) are taken from the following website: www.quantum-espresso.org/pseudopotentials/original-qe-pp-library/
20. A. Rappe, K. Rabe, E. Kaxiras and J. Joannopoulos, *Phys. Rev. B,* 1990, **41**, 1227(R).

21. J. Perdew, K. Burke and M. Ernzerhof, *Phys. Rev. Lett.,* 1996, **77**, 3865 (1996).
22. N. Marzari, D. Vanderbilt, A. De Vita and M. C. Payne, *Phys. Rev. Lett., 1999,* **82**, 3296.
23. H. Monkhorst and J. Pack, *Phys. Rev. B*, 1976, **13**, 5188.
24. S. Grimme, *J. Comput. Chem.*, 2006, **27**, 1787.
25. V. Barone, M. Casarin, D. Forrer, M. Pavone, M. Sambi and A. Vittadini, *J. Comput. Chem.*, 2009, **30**, 934.
26. N. Asschroft and N. Mermin, in: "Introduction to Solid State Physics", 5th ed., Saunders College, 1976.
27. Y. Gamo, A. Nagashima, M. Wakabayashi, M. Terai and C. Oshima, *Surf. Sci.,* 1997, **374**, 61.
28. W. Zhao, S. Kozlov, O. Höfert, K. Gotterbarm, M. Lorentz, F. Viñes, C. Papp, A. Görling and H. Steinrück, *J. Phys. Chem. Lett.,* 2011, **2**, 759.
29. F. Ortmann, F. Bechstedt and W. Schmidt, *Phys. Rev. B,* 2006, **73**, 205101.
30. I. Hamada and M. Otani, *Phys. Rev. B,* 2010, **82**, 153412.
31. M. Dion, H. Rydberg, E. Schrøder, D. Langreth and B. Lundqvist, *Phys. Rev. Lett.,* 2004, **92**, 246401.
32. K. Lee, E. Murray, L. Kong, B. Lundqvist and D. Langreth, *Phys. Rev. B*, 2010, **82**, 081101(R).
33. V. Cooper, *Phys. Rev. B*, 2010, **81**, 161104(R).
34. N. Troullier and J. Martins, *Phys. Rev. B*, 1991, **43**, 1993.
35. A. Castro Neto, F. Guinea, N. Peres, K. Novoselov and A. Geim, *Rev. Mod. Phys.*, 2009, **81**, 109.
36. J. Demaison and G. Wlodarczak, *Structural Chemistry*, 1994, **5**, 57.
37. Z. Yang, Q. Wang, X. Shan, S. Yang, H. Zhu, *Phys. Chem. Chem. Phys.*, 2014, **16**, 19654.